CHARACTERISTICS OF THE LINEAR POLARIZATION OBSERVED IN THE 16 MAY 1991 SOLAR FLARE

N.M. FIRSTOVA and A.V. BOULATOV
Institute of Solar-Terrestrial Physics (ISTP), P.O.Box 4026, Irkutsk, 664033, Russia
Internet: bulat@sitmis.irkutsk.su

Abstract. In a search for linear polarization effects, 37 profiles of the H_α line emitted in the 16 May 1991 flare have been analyzed. Linear polarization is clearly present in the central part of line. On average, the degree of polarization is 7 % , but it reaches 20 % in regions with lower H_α emission. Generally the orientation of the plane of polarization coincides with the flare to disk center direction, except for sections where the H_α line has the characteristic form observed in moustaches. We believe that the linear polarization observed in the 16 May 1991 flare was caused by bombardment of the chromosphere by beams of accelerated particles, protons in the main part of the flare and electrons at locations where the H_α line has the characteristic moustache structure.

Key words: Polarization – Flare

1. Introduction

Observation of the linear polarization of spectral lines in solar flares provides unique information on the modes of energy transfer from the corona to the chromosphere during solar flares, and significant properties of the energy transfer process can be derived from the measurement of the line emission polarization vector (Chambe and Hénoux, 1979; Hénoux and Semel, 1981; Hénoux *et al.*, 1983a; Hénoux and Chambe, 1990a; Smith *et al.*, 1990; Aboudarham *et al.*, 1992).

The first observations of impact linear polarization integrated over the profile of the 1437Å SI line in solar flares were made by Hénoux *et al.* (1983b) using the UVSP SMM spectropolarimeter. Observations of linear polarization in the H_α line in flares made with a narrow-band filter were published by Chambe and Hénoux (1979), Hénoux *et al.* (1990b) and Hénoux (1991), and observations of the linear polarization across the H_α line profile were published by Babin and Koval (1983, 1985a,b,c) and Kazantsev *et al.* (1991, 1993). The observed linear polarization cannot be caused by Zeeman or Stark effects. According to Hénoux and Semel (1981), the combination of these two effects, integrated over the H_α line profile, does not exceed 0.5%. Moreover, the wavelength dependence across the H_α line profile of the linear polarization must show the characteristic signatures associated with the Zeeman π and σ components; the observed H_α line polarization profiles do not show such signatures.

Solar Physics **164**: 361–372, 1996.

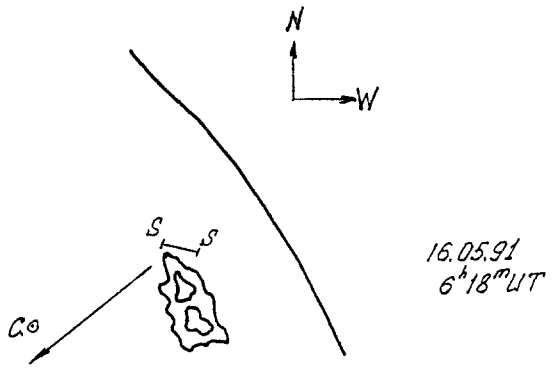

Fig. 1. A sketch of the active region No.6619. *SS* is the spectrograph slit position. The arrow indicates the direction towards the center of the solar disk.

Linear polarization is found in approximately 30 % of the observed H_α flare spectra. Normally the degree of polarization reaches 3-5 % , but in some cases it exceeds 10 % . In many cases the highest polarization signal is not observed in the brightest regions of the flare. The direction of the plane of polarization in flares basically coincides with the flare to disk center direction. As shown in Hénoux (1991), the analysis of other independent observations leads to the conclusion that the observed polarization is caused by the bombardment of the chromosphere either by proton beams (with a minimum energy for an individual proton at the coronal acceleration site of 200 keV) or by neutral beams.

Despite significant progress in the observation of impact linear polarization during the last decade, only a few observations have been made. In the present paper we present new observations of linear polarization in the H_α line in a flare observed on 16 May 1991 with the Baikal solar vacuum telescope. The spectrograms have been processed with a CCD in order to find the orientation and the spatial dependence of the polarization vector.

2. Observational data

2.1. Description of the observations

Our observations of the 16 May 1991 solar flare in the active region No. 6619 SGD (32N56W) were made with the Baikal solar vacuum telescope of ISTP (Skomorovsky and Firstova, 1995), using a $\lambda/2$-plate and a Wollaston prism inserted behind the spectrograph slit. The flare occured north-west of a large sunspot and was observed from 06:18 UT to 06:20 UT during a break in the clouds. Unfavorable weather conditions precluded the determination of the flare duration and importance. Figure 1 shows a sketch of active region No.

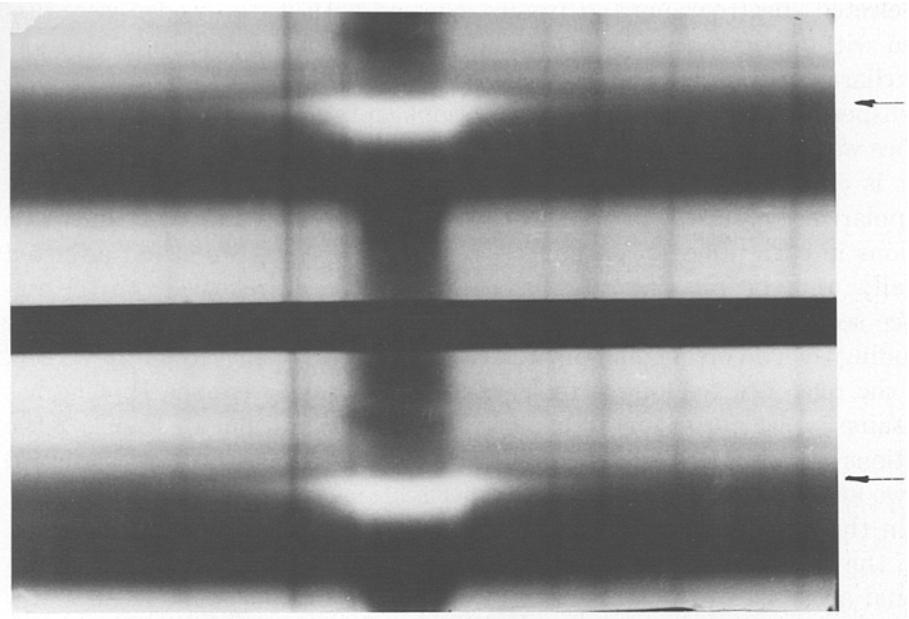

Fig. 2. A flare spectrogram in two orthogonal directions of polarization.

6619 in white light together with the spectrograph slit position at the time of recording and the flare to disk center direction.

The spectra were exposed for different positions of the $\lambda/2$-plate with one of the main axis of the plate making an angle with the direction of the spectrograph slit of 0°, 22.5° and 45°. These positions correspond respectively to the measurement of the Stokes parameters Q, U and $-Q$. This cycle was subsequently repeated. A total of 12 spectrograms were obtained, each of which consisting of two orthogonally polarized spectral bands. Figure 2 shows a photograph of one of the spectrograms. The height of an individual spectral band is 45 arcsec. Unfortunately the first frame was defocused, and the last six were overexposed. For that reason, only five frames, from the second to the sixth, were fully analysed.

2.2. Technique of analysing spectrograms with a CCD array

The photographic spectrograms were analysed with a CCD system installed at the telescope in 1993. For this purpose, a computer program was developed for constructing the characteristic curve, determining the dispersion, converting photographic densities to intensities, determining the H_α line center, calculating line profiles in units of the continuous spectrum, and for computing the polarization as a function of wavelength.

Selected spectrograms and frames exposed with a step wedge were digitized with a constant gain factor and with the same signal build-up time. The characteristic curve was constructed using these frames. Subsequently the dispersion averaged over several sections and common to all spectrogram frames was determined using reference lines.

It is crucial that the extracted H_α line profiles from the two orthogonal polarization states correspond to the same area on the solar disk. The sections in each polarization band serving as references were first adjusted visually, and the remaining sections were then fixed relatively to the reference sections. In order to adjust the reference sections, the whole frame including the two orthogonal polarization states was displayed on the screen, and the reference sections were selected at locations were the H_α line has the same typical form for both directions of polarization. In Figure 2 the positions of the reference sections in the two spectral bands are indicated by two arrows. The positions of the other sections were determined by moving in the direction of the spectrograph slit by an equal number of pixels from the location of the reference sections in the two bands. Thus the positional accuracy of the sections for the two orthogonal polarization states depends only on the precision with which the reference sections have been adjusted.

The beginning of each wavelength scan was selected in order to be as far as possible from the H_α center, and the value of the continuum was assigned to the first five points. Subsequently densities were converted to intensities that were normalized to the value of the continuum. The procedure was then repeated for every pair of associated sections for each given frame. As a result we obtained for each section for a set of wavelength positions relative to the line center, $\pm\Delta\lambda$, the H_α line intensities normalized to the continuum $I_1 = J_1/J_{cont}$ and $I_2 = J_2/J_{cont}$ in the first and second orthogonally polarized spectral bands as well as the values of Q/I or U/I given by

$$Q/I \text{ or } U/I = \epsilon(I_1 - I_2)/(I_1 + I_2), \tag{1}$$

where $\epsilon = \pm 1$ depending on the orientation of the $\lambda/2$-plate.

2.3. Observational accuracy

Accurate polarization observations require knowledge of the instrumental polarization. In addition to the first $\lambda/2$ plate installed in front of the spectrograph slit, a second $\lambda/2$ plate was placed behind the Wollaston prism, so that the electric vector of the ordinary and extraordinary rays would be at 45° with respect to the grating rulings. In the absence of the first retarder, the second $\lambda/2$-plate was adjusted by visually balancing the intensities of the quiet sun in the two spectral bands. If instrumental polarization were present it would have been impossible to balance the intensities. Furthermore, to improve the accuracy, all measurements of line intensities were

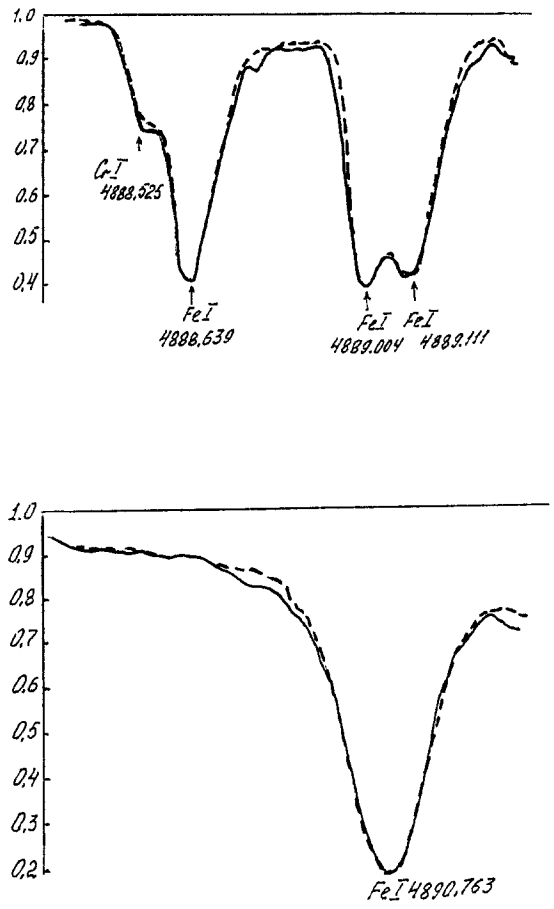

Fig. 3. Fe I and Cr I line profiles in a quiet region for two orthogonal polarization states.

usually normalized to the continuous spectrum. Figure 3 illustrates profiles of a few unpolarized Fe I and Cr I lines in a quiet region in the two spectral bands. We observe these lines under the same conditions as the H_α spectra, but the solar image was defocused and there should be no intrinsic polarization. A comparison of these lines in the two orthogonal polarization states provides evidence for the absence of instrumental polarization. It is worth noticing that the intensity of the continuous spectrum in the two spectral bands also remained unchanged when inserting the first $\lambda/2$-plate.

The differences that are seen in the line profiles for the two orthogonal polarization states in Figure 3 can be attributed to normal uncertainties of the photographic method. A considerable uncertainty is also present because of the difficulty of adjusting the reference sections. Once they are well adjusted the error in the line intensity between different frames varies from 1% to 8%.

3. Stokes parameters across the H_α line profiles

As mentioned above, five spectrograms taken in an interval of two minutes were processed. The recorded Stokes parameters in these spectrograms were as follows: I (U), II ($-Q$), III (Q), IV (U) and V ($-Q$). In each spectrogram, eight sections across the spectrograph slit were selected. The value $0''$ was assigned to the reference section, and the relative positions of the remaining sections were expressed in arcsec. Figure 4 shows H_α profiles for the two orthogonal polarization states for the section $-3.75''$ in each of the five spectrograms. The solid line shows the H_α profile for the first polarization state, the dashed line corresponds to the second.

In the case of simultaneous exposure of the five spectrograms, the relative intensity variation in the two spectral bands of Figure 4.III (Q) should be opposite to that of Figure 4.II and 4.V ($-Q$), since the direction of polarization has changed by 90°. This is also what we find, although image motion and intrinsic time variations could have affected the results, since the exposures were not simultaneous. Figure 4 shows the predominance of linear polarization along the slit, rather than along the dispersion direction.

The profiles in Figure 4 were obtained by one recording. Since all sections were recorded twice or three times, the H_α line intensity profiles for each section were averaged and smoothed with the formula

$$I_{k,j} = (I_{k,j} + \frac{2}{3}(I_{k,j-1} + I_{k,j+1}) + \frac{1}{3}(I_{k,j-2} + I_{k,j+2}))/3\,, \qquad (2)$$

where $k = 1,2$ is the index of the polarization band, and j is the index of the wavelength coordinate. Figure 5 presents, for spectrogram III, averaged values of I_1 and I_2 in all sections across the spectrograph slit, as well as of the parameter Q/I for these sections. The horizontal bar corresponds to the zero level of the Q/I parameter.

The most systematic behavior of the Stokes parameters is observed at line center. Therefore the data were analyzed in two wavelength ranges around the line center: -1 Å$< \Delta\lambda <+1$Å and -0.5Å$< \Delta\lambda <+0.5$Å. Figure 6a shows the behavior of the mean intensity of the H_α line in the interval -1Å$< \Delta\lambda <+1$Å for the five exposures. The positions of the flare portions along the spectrograph slit are given in arcsec. Figure 6b gives the quantities Q/I, U/I and $-Q/I$ in the same interval; the errors are marked by vertical bars. Crosses show mean values of the Stokes parameters in the wavelength range -0.5Å$< \Delta\lambda < +0.5$Å. To compare time-adjacent values of the Q parameter, the plot in Fig. 6bIII includes the values from Fig. 6bII with reversed sign.

By comparing the Stokes parameters for different spectrograms, the following features emerge. Spectrograms I and IV (Stokes U) agree reasonably well in a relatively quiet region (sections $0''$ – $5''$) but are in rather poor

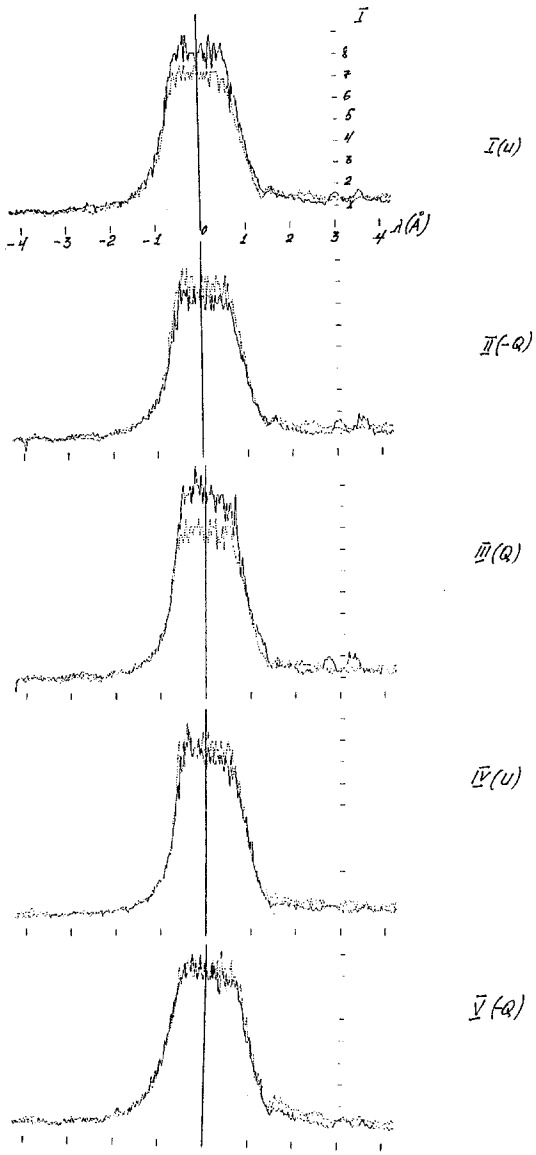

Fig. 4. H_α profiles in the two orthogonal polarization states for the section $-3.75''$ for different orientations of the entrance $\lambda/2$-plate. The full line and dotted line profiles correspond respectively to the directions of polarization numbered 1 and 2 in Eq. (1). Using this equation with $\epsilon = 1$, they provide the Stokes parameters U, Q or -Q.

agreement in the emission part of the flare. As far as Stokes Q is concerned, the situation is the opposite: rather good agreement between $-8''$ and $0''$, and a very strong spread of the values in the relatively quiet region ($0''$ – $5''$).

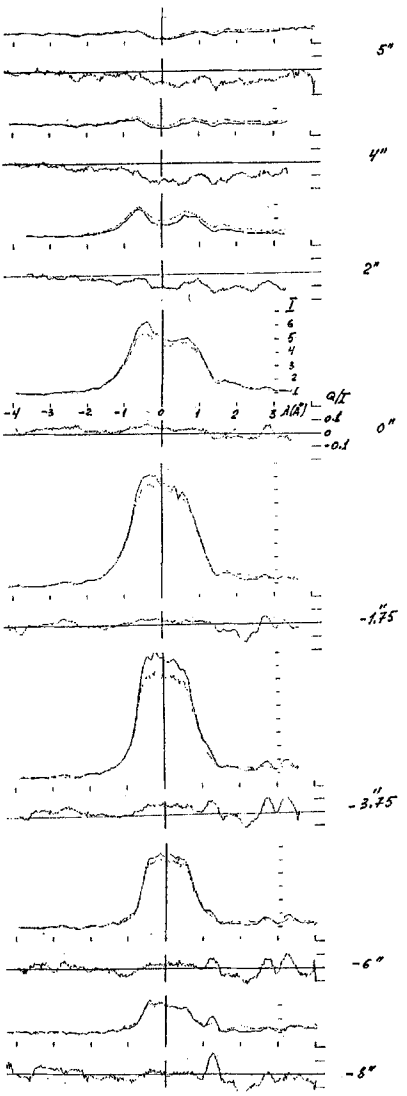

Fig. 5. H_α intensity and Stokes Q profiles for spectrogram III in all sections at various positions along the spectrograph slit.

4. Orientation and amplitude of the polarization vector

To derive the final results, spectrograms IV and V were dismissed, since they were of lower quality. Spectrograms I–III were used to determine the mean intensity of the flare emission along the spectrograph slit. The degree

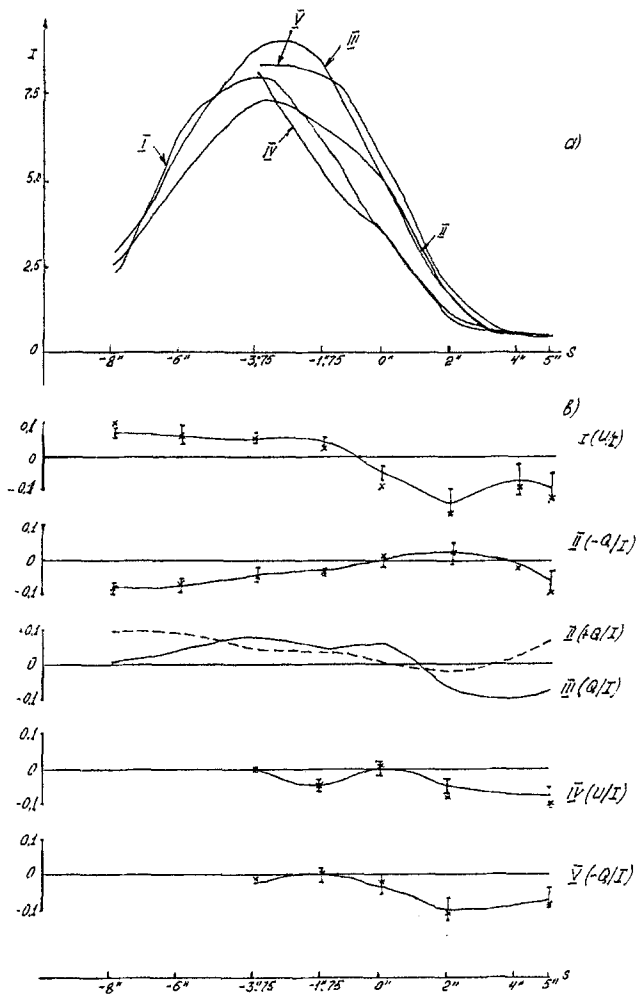

Fig. 6. Variation along the spectrograph slit of the mean H_α intensity (a) and of the mean values of Q/I, $-Q/I$ and U/I (b). Averaging has been made over the interval $-1\text{Å} < \Delta\lambda < +1\text{Å}$. Crosses show mean values averaged over the interval $-0.5\text{Å} < \Delta\lambda < +0.5\text{Å}$.

of polarization P and the azimuth χ of the polarization plane relatively to the direction of the spectrograph entrance slit are given by

$$P = \sqrt{\frac{Q^2}{I^2} + \frac{U^2}{I^2}} \quad \text{and} \quad \cot 2\chi = Q/U\,. \tag{3}$$

We used spectrograms II, III (providing Stokes Q) and I (Stokes U) to calculate P and χ.

Figures 7a,b,c show a three-dimensional image of I, P and χ versus the wavelength and section number. In spite of multiple averaging and smoothing, the degree of polarization and, to a much larger extent, the polarization

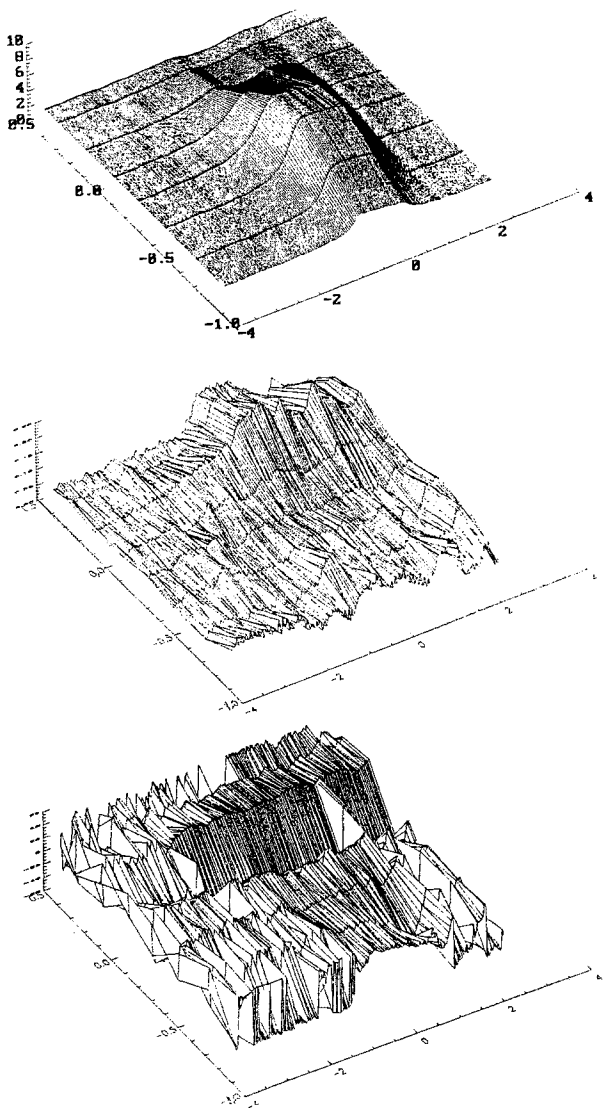

Fig. 7. Three-dimensional representation of I (a), P (b) and χ (c) versus the wavelength and flare position along the spectrograph slit (section number).

azimuth, show a significant spread along the dispersion direction, especially in the line wings.

Figure 8 gives P and χ for the central portion of the H_α line; the photometric section with the intensity at H_α line center along the spectrograph slit is also included. The length of each line segment is proportional to P, and its direction is given by the angle χ. The polarization pattern at the

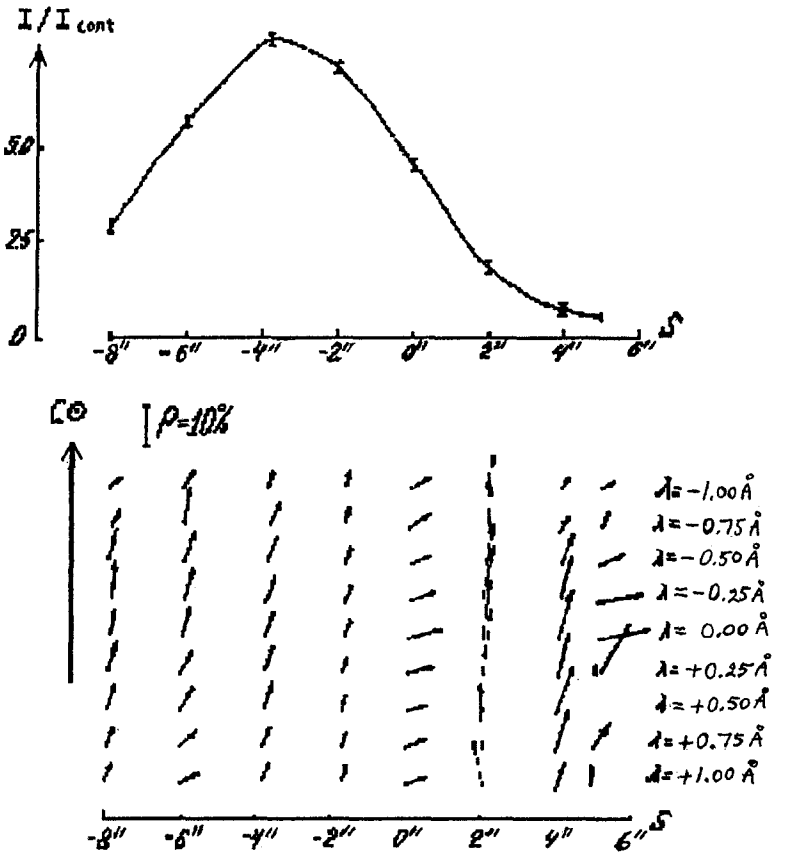

Fig. 8. Linear polarization vector in different sections and in different portions of the central part of the H_α line. The upper curve shows the intensity variation at the H_α line center. The arrow is directed towards the center of the solar disk.

H_α line center is well defined. In sections with high emission (from $-8''$ to $-1.75''$) the polarization vector is generally close to the direction towards the center of the solar disk, and the degree of polarization drops from 8% in section $-8''$ to 4% in section $-1.75''$. In section $0''$, where the H_α emission profile resembles moustaches, the degree of polarization increases again, and the polarization vector is oriented almost perpendicular to the direction toward the center of the solar disk. Moreover, in section $2''$ where the shape of the H_α profile also resembles moustaches, and in sections $4''$ and $5''$, which correspond to an almost unperturbed photosphere, the value of the degree of polarization increases substantially and reaches 20%. The direction of the polarization vector in sections $4''$ and $5''$ is close to the flare to disk center direction. The r.m.s. error of P and χ are 0.007 and 4°, respectively, for sections within $-6''$ and $+2''$. In section $8''$ and especially in sections $4''$ and $5''$, this error is much larger.

5. Conclusions

The degree of polarization observed in the 16 May 1991 flare is on average 7%, and it reaches 20% in regions with weaker emission and in adjacent areas of the weakly perturbed chromosphere. The plane of polarization is parallel to the direction of the centre of the solar disk. The observed linear polarization vector can be explained (cf. Hénoux, 1991) by bombardment of the chromospheric hydrogen atoms by proton or neutral particle beams.

At flare locations where the shape of the H_α line profile reminds of moustaches (sections 0″ and 2″), the direction of the plane of polarization is mainly tangential (perpendicular to the flare to disk center direction). The H_α profiles in these sections agree with calculated H_α profiles excited by accelerated electrons bombarding the chromosphere (Fang *et al.*, 1993), while the H_α line in other parts of the flare corresponds more to profiles, calculated for excitation by proton beams (Hénoux *et al.*, 1993).

Thus we believe that the observed linear polarization in the flare was caused by bombardment of the chromosphere by accelerated particles: protons in the main part of the flare, and electrons in those flare regions, where the H_α line has the shape of a moustache profile.

References

Aboudarham, J., Berrington, K., Callaway, J., Feautrier, N., Hénoux, J.C., Peach, G., and Saraph, H.-E.: 1992, *Astron. Astrophys.* **262**, 302-307.
Babin, A.N., Koval, A.N.: 1983, *Izvest. KrAO* **66**, 89-102.
Babin, A.N., Koval, A.N.: 1985a, *Izvest. KrAO* **72**, 142-153.
Babin, A.N., Koval, A.N.: 1985b, *Izvest. KrAO* **79**, 3-8.
Babin, A.N., Koval, A.N.: 1985c, *Solar Phys.* **98**, 159-161.
Chambe, G., Hénoux, J.C.: 1979, *Astron. Astrophys.* **80**, 123-129.
Fang, C., Hénoux, J.C., Gan, W.Q.: 1993, *Astron. Astrophys.* **274**, 917-922.
Hénoux, J.C., Semel, M.: 1981, *God Solnechnogo Maksimuma*, **1**, 207-210.
Hénoux, J.C., Chambe, G., Heristchi, D., Semel, M., Woodgate, B., Shine, R., Beckers, J.: 1983a, *Solar Phys.* **86**, 115-122.
Hénoux, J.C., Chambe, G., Semel, M., Sahal, S., Woodgate, B., Shine, R., Beckers, J.: 1983b, *Astrophys. J.* **265**, 1066-1075.
Hénoux, J.C., Chambe, G.: 1990a, *J. Quant. Spectrosc. Radiat. Transfer* **44**, 193-201.
Hénoux, J.C., Chambe, G., Smith, D.F., Tamres, D., Feautrier, N., Rovora, M., Sahal-Brechot, S.: 1990b, *Astrophys. J. Suppl. Ser.* **73**, 303-311.
Hénoux, J.C.: 1991, in L.J. November (ed.), *Solar Polarimetry*, NSO/SP Summer Workshop Series No. **11**, 285-295.
Hénoux, J.C., Fang, C., Gan, W.Q.: 1993, *Astron. Astrophys.* **274**, 923-930.
Kazantsev, S.A., Firstova, N.M., Gubin, A.V., Lankevich, N.A.: 1991, *Optika i Spektroskopiya* **70**, 990-995.
Kazantsev, S.A., Petrashen, A.G., Firstova, N.M., Hénoux, J.C.: 1993, *Optika i Spektroskopiya* **75**, 644-657.
Skomorovsky, V.I., Firstova, N.M.: 1995, *Solar Phys.* , in press.
Smith, D.F., Chambe, G., Hénoux, J.C., Tamres, D.: 1990, *Astrophys. J.* **358**, 674-679.